Gap domain wall fermions

Pavlos M. Vranas[*]

IBM T. J. Watson Research Center, Yorktown Heights, New York 10598, USA
(Received 3 July 2006; published 23 August 2006)

I demonstrate that the chiral properties of domain wall fermions (DWF) in the large to intermediate lattice spacing regime of QCD, 1 to 2 GeV, are significantly improved by adding to the action two standard Wilson fermions with supercritical mass equal to the negative DWF five-dimensional mass. Using quenched DWF simulations I show that the eigenvalue spectrum of the transfer matrix Hamiltonian develops a substantial gap and that the residual mass decreases appreciatively. Furthermore, I confirm that local topology changing remains active and that the hadron spectrum of the added Wilson fermions is above the lattice cutoff and therefore is irrelevant. I argue that this result should also hold for dynamical DWF and furthermore that it should improve the chiral properties of related fermion methods.

PACS numbers: 11.15.Ha, 11.30.Rd, 12.38.Gc

I. INTRODUCTION

Domain wall fermions (DWF) and other closely related methods provide the most faithful lattice regularization of QCD with unprecedented chiral symmetry and topological properties. These methods have produced an impressive wealth of results and have brought about a new and brave era for lattice gauge theory. Several proposals for improvement have also been demonstrated. The reader is referred to the reviews [1–9], related works [10], and references therein for more details. Here I will focus on DWF and QCD. The method I will describe should apply to all closely related lattice fermions as well as to other gauge theories similar to QCD (such as $\mathcal{N} = 1$ Super Yang-Mills [11]). The method was first proposed in [1].

Using the new generation supercomputers and numerical simulation algorithms, one can now simulate dynamical QCD at zero and finite temperature in the strong to intermediate coupling regime with lattice spacing a in the region 1 GeV $\lesssim a^{-1} \lesssim 2$ GeV and for the number of lattice points L_s along the fifth dimension in the neighborhood of $L_s \approx 20$ to 100 depending on the lattice spacing a. These L_s values are now certainly within the reach of the latest supercomputers. However, one obviously would like to do better. A method that would improve DWF so that smaller values of L_s are needed would be very welcomed, not only for the obvious benefits in computing time but also as a matter of theoretical interest. The reasons behind the need for rather large values of L_s are as involved as they are interesting. But they are also a lattice artifact. It should be possible to remove it without spoiling the important features of DWF.

In this work I demonstrate that the chiral properties of DWF in the large to intermediate lattice spacing regime 1 GeV $\lesssim a^{-1} \lesssim 2$ GeV are significantly improved by adding to the action two standard Wilson fermions with mass equal to the negative DWF five-dimensional mass m_0

(Wilson supercritical region). These fermions produce a fermion determinant that is identically zero when the fifth dimension transfer matrix Hamiltonian $H_4(m_0)$ has a zero. Therefore, small eigenvalues of $H_4(m_0)$ ought to be suppressed in the simulation. It is precisely these eigenvalues that are a lattice artifact and are directly responsible for the large L_s requirement. Suppressing them allows one to achieve the same chiral symmetry restoration for smaller values of L_s. Indeed, I show that the eigenvalue spectrum of $H_4(m_0)$ develops a substantial *gap* and that the residual mass m_{res}, quantifying the remnants of chiral symmetry breaking, decreases appreciatively. I use this key property to name this fermion regulator as gap domain wall fermions (GDWF). For other DWF related fermions (for example overlap-Neuberger fermions) I argue that this method of adding gap fermions (GF) should also improve their chiral properties.

In order to make sure there are no adverse "side effects," I confirm that local topology changing (measured using the overlap index method) remains active; instantons and anti-instantons with size larger than a lattice spacing are active appearing and disappearing in the gauge field configurations (note that this does not necessarily imply that the net index is changing). Also, I confirm that the hadron spectrum of the added Wilson fermions is above the lattice cutoff and therefore is irrelevant. Furthermore, I check that parity is not broken and therefore the added Wilson fermions are well outside the Aoki phase. All numerical simulations in this work were performed on 512-node IBM BlueGene/L supercomputers.

This paper is organized as follows: In Sec. II, DWF and the difficulties with chiral restoration are briefly reviewed. In Sec. III, the GDWF method is presented. In Sec. IV, numerical results using GDWF in the quenched approximation on $16^3 \times 32$ lattices are given for three lattice spacings $a^{-1} \approx 1.0$, 1.4, and 2.0 GeV, and are compared with the quenched approximation of standard DWF at the same lattice spacings. Also, in this section I argue that these results will hold for dynamical GDWF as well. In

*Electronic address: vranasp@us.ibm.com

034512-1

Sec. V, an example of a quenched two-flavor QCD simulation with GDWF at the rather large lattice spacing $a^{-1} \approx$ 1.4 GeV is presented. It is shown that the pion mass acquires physical values already for an L_s as small as 24 with m_{res} contributing about 10% to the bare quark mass. In Sec. VI I discuss issues that relate to topology. In Sec. VII, the ease of implementing GDWF, as well as the small GDWF computational cost added to the cost of a DWF simulation, is discussed. In Sec. VIII, some curious theoretical thoughts brought up by GDWF are pondered upon. In Sec. IX, I discuss the applicability of the method to overlap and Neuberger fermions and furthermore to the $\mathcal{N} = 1$ Super Yang-Mills theory. Also, I present open issues for further exploration. The conclusions are given in Sec. X.

II. DWF AND THE CHIRAL RESTORATION PROBLEM

Lattice DWF [12–16] are defined in five dimensions. The fifth dimension has L_s lattice sites and the five-dimensional fermion has positive bare mass m_0 (domain wall height). The five-dimensional Dirac operator D_F employs free boundary conditions at the edges of the fifth dimension (walls). As a result, the plus chirality fermionic components are localized on one wall while the minus chirality components are localized on the other. The two chiralities are explicitly mixed with a mass parameter m_f. The gauge fields are defined in four dimensions only. They

are the same along the fifth dimension and have no fifth component. This allows for a definition of a transfer matrix T along the fifth direction that is the same in all "slices" along that direction. The product of the transfer matrices along the fifth direction is therefore T^{L_s}. The single particle Hamiltonian $H_4(m_0)$ associated with this transfer matrix is then also independent of the fifth dimension. It is defined in four dimensions and, for the case where the fifth dimension is continuous, one can show that $H_4(m_0) = \gamma_5 \slashed{D}_w(-m_0)$ where $\slashed{D}_w(-m_0)$ is the standard Wilson fermion Dirac operator with mass $-m_0$. When the fifth dimension is not continuous the Hamiltonian has a more complicated form, but one can show that it has the same zero eigenvalues as $H_4(m_0)$.

The five-dimensional Dirac operator is given by the equation:

$$D_F(x, s; x', s'; m_0, m_f) = \delta(s - s')\slashed{D}(x, x'; m_0)$$
$$+ \slashed{D}^\perp(s, s'; m_f)\delta(x - x'; m_f) \quad (1)$$

$$\slashed{D}(x, x'; m_0) = \frac{1}{2}\sum_\mu [(1 + \gamma_\mu)U_\mu(x)\delta(x + \hat{\mu} - x')$$
$$+ (1 - \gamma_\mu)U_\mu^\dagger(x')\delta(x' + \hat{\mu} - x)]$$
$$- (4 - m_0)\delta(x - x') \quad (2)$$

$$\slashed{D}^\perp(s, s'; m_f) = \begin{cases} P_R\delta(1 - s') - m_f P_L\delta(L_s - 1 - s') - \delta(0 - s') & s = 0 \\ P_R\delta(s + 1 - s') + P_L\delta(s - 1 - s') - \delta(s - s') & 0 < s < L_s - 1 \\ -m_f P_R\delta(0 - s') + P_L\delta(L_s - 2 - s') - \delta(L_s - 1 - s') & s = L_s - 1 \end{cases} \quad (3)$$

$$P_{R,L} = \frac{1 \pm \gamma_5}{2}, \quad (4)$$

where m_0 is the five-dimensional mass representing the "height" of the domain wall and m_f is the explicit bare quark mass. The gamma matrices γ are taken in the chiral basis.

The standard Wilson fermion Dirac operator is

$$\slashed{D}_w(x, x'; -\mu) = \slashed{D}(x, x'; \mu). \quad (5)$$

The localization of the two chiral components on the opposite walls is exponentially good. The slowest decay coefficient is proportional to the smallest, in absolute value, negative eigenvalue of $H_4(m_0)$. For infinite L_s (overlap fermions) the two chiralities completely decouple provided that $H_4(m_0)$ does not have eigenvalues that are exactly zero. That possibility is of measure zero and is therefore of no concern. Nevertheless, at finite L_s, where simulations are performed, the two chiralities will mix and break chiral symmetry. Furthermore, if $H_4(m_0)$ has very small eigenvalues the exponential decay will be overshad-

owed by slow power law decay even for very large L_s. This mixing is of a similar nature as the one produced by a mass term. It is possible to calculate this "effective" mass (usually called residual mass, m_{res}) and use it to quantify the quality of the DWF regulator. Clearly, at finite L_s one would like $H_4(m_0)$ to have a substantial gap which in turn would result to a rapidly decreasing m_{res} as L_s is increased.

Obviously the spectrum of $H_4(\mu)$ at various values μ is of particular importance. A small review is given below. It will serve to explain GDWF. The reader is referred to the original work [13] for more details. For any gauge field configuration $H_4(\mu)$ has the same number of positive (n_+) and negative (n_-) eigenvalues for $\mu < 0$. However, as μ is increased above zero some eigenvalue of $H_4(\mu)$ may cross zero and change sign. Then $n_+ - n_-$ would not be zero just after the crossing occurs. It has been shown that the number and direction of crossings is directly related to the number of instantons and anti-instantons present in the gauge configuration [13,17] and that $n_+ - n_-$ is in fact equal, in a statistical sense, to the net (global) topological charge of the gauge field configuration [18]. The Atiyia-

Singer index theorem is realized on the lattice in a statistical sense. These are rather remarkable properties.

A very nice way to look at the spectrum of $H_4(\mu)$ is to plot the eigenvalues of $H_4(\mu)$ as a function of μ. This is an eigenvalue flow diagram [13,17,18] (see Fig. 4). Instantons that are larger than the lattice spacing are of course of physical interest and it has been shown [17] that they produce crossings in rather localized neighborhoods of μ that correspond to the edges of the standard Brillouin zones. For a single flavor DWF, one picks $\mu = m_0$ in-between the first and second set of crossings. Since this is a finite range no fine-tuning is required. In the continuum limit the range for one flavor extends from 0 to 2 and the width of the neighborhoods where crossings occur tends to zero. The location and width of the crossing neighborhoods is renormalized from their continuum values as the coupling is made stronger. For example, for lattice spacing $a^{-1} \approx 1.4$ GeV, the first set of crossings occur in the neighborhood of $\mu_{\min} \approx 0.9$ and the second in the neighborhood of $\mu_{\max} \approx 2.2$. Their width is approximately 0.2. However, small instantons of the size of the lattice spacing are generated/destroyed because they can "come up/fall in" through the discrete lattice. This generates additional crossings throughout the $\mu_{\min}$, $\mu_{\max}$ region.

In a numerical simulation at small lattice spacing (weak coupling) there are few to no such small instanton crossings. The simulation is performed at a $\mu = m_0$ in the middle of the relevant range. At that value, since there are no crossings, the eigenvalue gap is large and therefore the localization on the walls is good. As a result, the two chiralities mix very weakly and break chiral symmetry minimally (as a result m_{res} decreases rapidly with increasing L_s). However, at large lattice spacings (strong coupling) the small instantons generate crossings across the whole range and therefore also close to m_0. As a result the eigenvalue gap becomes very small. To be sure the probability of an eigenvalue crossing *exactly* at m_0 is zero. There is always a gap but it may be very small at large lattice spacings. The challenge is to suppress the crossings due to the lattice spacing size instantons, which are obviously an artifact of the lattice "discreteness," without destroying the crossings due to the all-important physical instantons with size of many lattice spacings.

III. GAP DOMAIN WALL FERMIONS

A method that would produce a sizable gap in the spectrum of $H_4(m_0)$ for lattice spacings in the $1 \text{ GeV} \lesssim a^{-1} \lesssim 2 \text{ GeV}$ region would be of great use. Here I describe such a method. Gap domain wall fermions are similar to standard domain wall fermions but they have the desired *gap*.

Since $H_4(m_0) = \gamma_5 D_w(-m_0)$ where $D_w(-m_0)$ is the standard Wilson fermion Dirac matrix, one can induce a larger gap by adding to the theory standard dynamical Wilson fermions with mass $-m_0$. Here I add two flavors. When integrated out these fermions contribute a factor of

$\det^2[D_w(-m_0)] = \det^2[H_4(m_0)]$ to the Boltzmann weight. Gauge field configurations for which $H_4(m_0)$ has small eigenvalues will be suppressed by this Boltzmann weight and therefore they will be sampled very infrequently. In particular, any gauge field configuration for which $H_4(m_0)$ has a zero eigenvalue is explicitly excluded (not to mention that the set of such configurations is of measure zero). But more to the point is the fact that this Boltzmann weight "repels" gauge configurations for which the gap at m_0 is small. One can expect a substantially larger gap even for strong couplings. In Sec. IV, I present numerical results that demonstrate that indeed this is the case. Notice that I have not added any extra parameters since the Wilson fermions have mass equal to the negative five-dimensional mass which is already a parameter of the theory.

The Wilson fermions that I added to the theory have mass $-m_0$ with m_0 somewhere in the middle of the crossings region $[\mu_{\min}, \mu_{\max}]$. I have chosen $m_0 = 1.9$ which is a good choice for the whole range of lattice spacings of interest. Such a mass is in the supercritical region of Wilson fermion masses and is very heavy. The hadron spectrum, including the pions, of these two flavors of Wilson fermions, should be above the cutoff. In that case their contribution to the low energy physics of the theory is irrelevant. Indeed, in Sec. IV, I present numerical results that demonstrate that their hadron spectrum is above the cutoff. Here it should be noted that for smaller lattice spacings than the ones I considered in this work the contribution of the heavy Wilson fermions should obviously remain irrelevant provided that m_0 is always chosen in the supercritical region. However, for larger lattice spacings than the ones considered here one should be cautious. With increasing lattice spacing the size of the supercritical region gets smaller and may be completely overtaken by the adjacent Aoki phase regions and therefore shrink to zero size. If this happens one cannot choose a value for m_0 in the supercritical region, the Wilson operator will have massless excitations and this method will not work. Here I do not investigate this case since such large lattice spacings are of no direct interest to current numerical simulations. In any case, I show that parity is not broken for the lattice spacings considered in this work and therefore the added Wilson fermions are well outside the Aoki phase.

As mentioned earlier, it is important that crossings due to the all-important physical instantons with size of many lattice spacings are present. The added Wilson fermions have mass $-m_0$ and they suppress the crossings around m_0 but have little effect further away. Because m_0 is chosen somewhere in the middle of the allowed range, the larger instanton crossings are not affected since they occur at the edges of the allowed range. Again, in Sec. IV, I present numerical results that demonstrate that this is the case.

The GDWF full partition function for QCD is given by

$$Z = \int [dU] \int [d\bar{X} dX] \int [d\bar{\Psi} d\Psi] \int [d\Phi^\dagger d\Phi] e^{-S}, \quad (6)$$

$U_\mu(x)$ is the gauge field, $X(x)$ is the four-dimensional Wilson fermion field, $\Psi(x, s)$ is the five-dimensional fermion field, and $\Phi(x, s)$ is the five-dimensional bosonic Pauli Villars (PV) type field. x is a coordinate in the four-dimensional space-time box with extent L along each of the directions, $\mu = 1, 2, 3, 4,$ and $s = 0, 1, \ldots, L_s - 1$, where L_s is the size of the fifth direction and is taken to be an even number. The action S is given by

$$
\begin{aligned}
S &= S(\beta, L, L_s, m_0, m_f) \\
&= S_G(U; \beta, L) + S_W(\bar{X}, X, U; -m_0, L) \\
&\quad + S_F(\bar{\Psi}, \Psi, U, m_0, m_f, L, L_s) \\
&\quad + S_{\text{PV}}(\Phi^\dagger, \Phi, U; m_0, L, L_s),
\end{aligned}
\tag{7}
$$

where S_G, is the standard plaquette Wilson gauge action with coupling g ($\beta = 6/g^2$) [19]. Of course, any pure gauge action can be chosen instead. In particular, one can choose a lattice gauge action that most closely resembles the continuum action. For example, a popular choice is the Iwasaki action [20]. Because, as mentioned above, DWF maintain a connection between their index and the topological charge, it is possible to improve them by suppressing small instantons by an appropriate choice of the lattice pure gauge action [1,3,21,22]. The Iwasaki-type actions have been shown to have this property but mostly for lattice spacings in the lower end of the interval considered here and below. In any case, in order to be able to evaluate GDWF alone I did not want the improvements due to these actions to obscure the results and that is why I use the standard Wilson gauge action. However, it should be obvious that for production simulations one should use an improved gauge action not only because of the possible additional improvement on the chiral properties but also because of the closer resemblance to the continuum gauge action. S_W is the standard Wilson fermion action [19] with mass $-m_0$. $S_F + S_{\text{PV}}$ is the standard domain wall fermion action with the Pauli Villars regulator, five-dimensional mass m_0 and explicit bare quark mass m_f [12–15].

IV. NUMERICAL RESULTS

In this section, I present numerical results that demonstrate the properties of GDWF.

Because of limited computational resources, I use the "quenched" approximation for the DWF sea fermions. However, unlike standard quenched simulations I consider large lattice spacings that are of interest to dynamical DWF simulations. I compare results obtained from simulations with no dynamical Wilson flavors with results obtained at the same lattice spacing with two dynamical Wilson flavors with mass $-m_0$. I use only one value of $m_0 = 1.9$ throughout this work. In order to compare results, I match the lattice spacing between the two cases by adjusting β. Here I achieve a 5% or better matching level at three values of the lattice spacing $a^{-1} \approx 1.0$ GeV, 1.4 GeV, and 2.0 GeV.

Measurements are done using the DWF operator at $m_0 = 1.9$. The space-time volume of all simulations is $16^3 \times 32$. More technical details about the numerical simulations are given in the Appendix.

Therefore, the two cases correspond to standard quenched DWF simulations and to quenched GDWF simulations. Again, the lattice spacings I use are large and of interest to dynamical simulations. I expect that the effects on chiral symmetry due to the DWF quenching are to a large extent taken into account by simulating at these large lattice spacings. To be sure the quenched approximation does not allow for the calculation of a systematic error. However, if previous results are of any guide, I expect that quenching may affect mass measurement results at the 10% level. Since the improvements observed here are at the 1 order of magnitude level, I do not expect that quenching is affecting the results in any significant way.

The first order of business is to match the lattice spacings between DWF and GDWF. I measure the ρ and nucleon masses at $L_s = 16$ and extrapolate to $m_f = 0$. The results for three values of β are shown in Fig. 1. These values of β were chosen so that the $m_f = 0$ extrapolated ρ masses match the quenched DWF masses of [23].

The matching for the $m_f = 0$ extrapolated masses is shown in Fig. 2. The DWF ρ masses match well (better than 5%). I choose the DWF $m_f = 0$ extrapolated ρ mass to set the scale. The values of β shown correspond to $a^{-1} \approx 1.0$ GeV, 1.4 GeV, and 2.0 GeV. The nucleon masses also match well (better than 5%) which is an indication that the method works properly. From now on, I will use these values of beta to perform comparisons of the chiral properties of DWF and GDWF. The inverse lattice spacing in GeV corresponding to the quenched GDWF β values is plotted in Fig. 3.

In Fig. 4 the ten smallest magnitude eigenvalues of $H_4(m_0)$ are plotted vs m_0. The eigenvalues are calculated with an accuracy 10^{-6} and are measured in m_0 steps of 0.025. An aggregate of the results from 20 independent configurations (separated by 20 configurations) is plotted in each plot. The left column is from 0-flavor Wilson simulations while the right column is from 2-flavor Wilson with mass $-m_0$. Horizontally, the 0-flavor and 2-flavor β values correspond to the same lattice spacing (Fig. 2). From top to bottom $a^{-1} \approx 1.0$ GeV, 1.4 GeV, and 2.0 GeV. Notice the difference in the y-axis scale for the different lattice spacings. The "crosshairs" indicate the $m_0 = 1.9$ point. One can clearly see that the 2-flavor Wilson fermions generate a substantial gap around m_0 where none existed before even at the large lattice spacing $a^{-1} \approx 1.0$ GeV.

Furthermore, it is very important to observe in Fig. 4 that the 2-flavor Wilson fermions generate the gap at a neighborhood of $m_0 = 1.9$, but allow for a copious amount of crossings at the edges of the allowed m_0 range. As mentioned in Sec. II, these crossings correspond to instantons
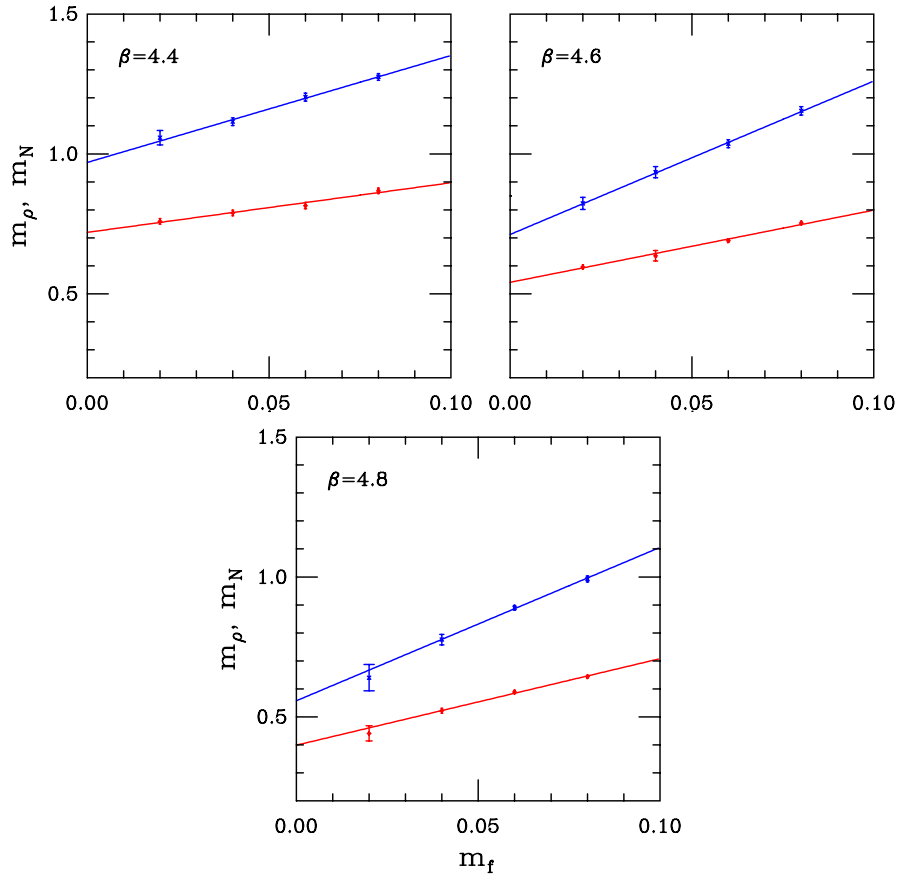
FIG. 1 (color online). The quenched GDWF nucleon (top points) and the rho (bottom points) mass in lattice units vs m_f at $L_s = 16$ for three values of β. The extrapolated $m_f = 0$ rho mass is used to set the scale.
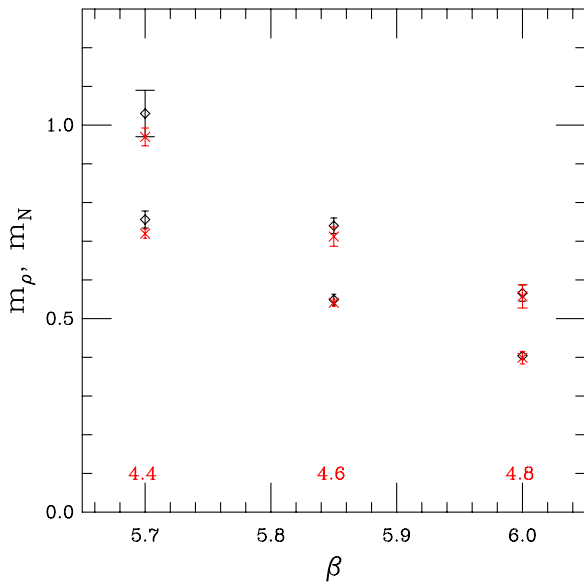

FIG. 2 (color online). Matching the scale of quenched GDWF with the scale of quenched DWF. The nucleon (top points) and the rho (bottom points) mass in lattice units for three values of β is shown. The diamonds are for DWF from Ref. [23] and the crosses are for GDWF. Also the β values for DWF are the bottom numbers of the x-axis while the GDWF β values are the top numbers of the x-axis.
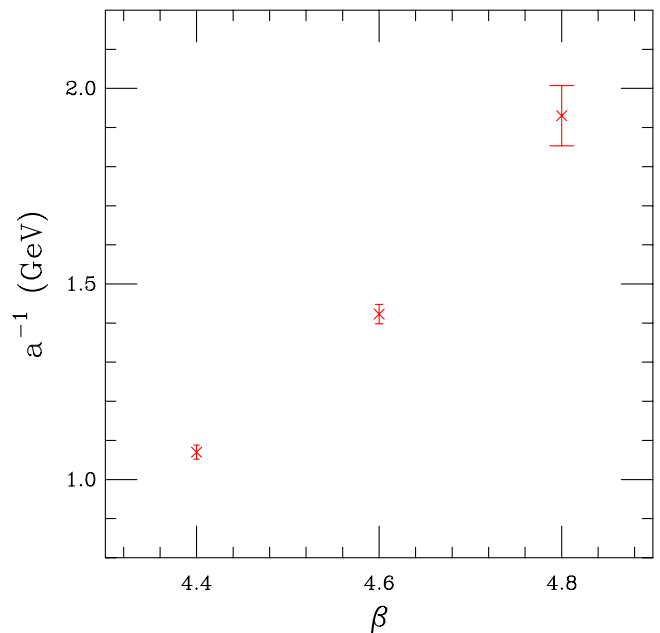

FIG. 3 (color online). The inverse lattice spacing in GeV vs the quenched GDWF β values used in this work.
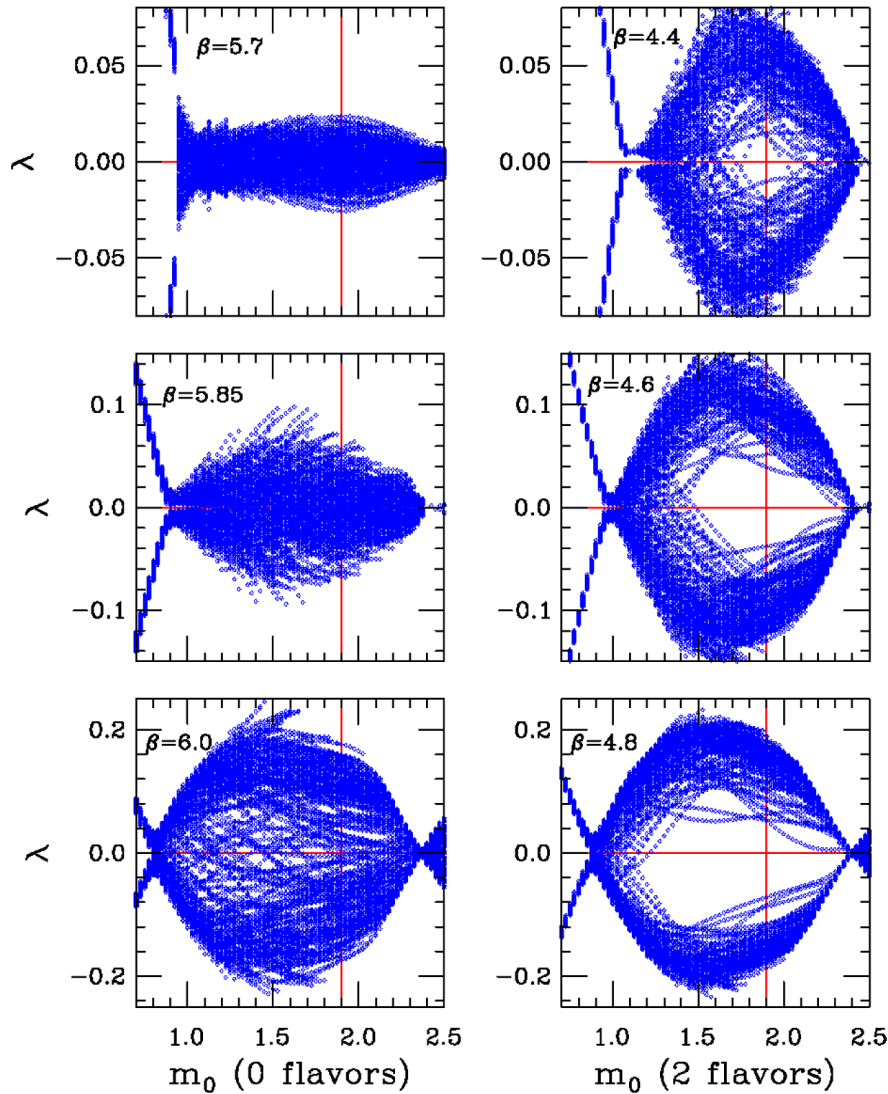
FIG. 4 (color online).   The ten smallest magnitude eigenvalues of $H_4(m_0)$ vs m_0. An aggregate of the results from 20 independent configurations is plotted in each plot. The left column is from 0-flavor Wilson (quenched) simulations while the right column is from 2-flavor Wilson with mass $-m_0$. Horizontally the 0-flavor and 2-flavor β values correspond to the same lattice spacing (Fig. 2). From top to bottom, $a^{-1} \approx 1.0$ GeV, 1.4 GeV, and 2.0 GeV. Notice the difference in the y-axis scale for the different lattice spacings.

with size larger than a lattice spacing and are of physical interest. Although Fig. 4 shows the cumulative results of 20 configurations, by close inspection I confirmed that the number of crossings changes from configuration to configuration. This indicates instanton, anti-instanton activity. However, with the current resolution, I am not able to measure the net topological index. This is beyond the scope of this work. For further discussion see Sec. VI.

In order to get a better picture of the small eigenvalue distribution I chose to look at the $m_0 = 1.9$ "cross section" for the 0 and 2 flavor cases at $a^{-1} \approx 1.4$ GeV ($\beta = 5.85$, 4.6) using a larger number of eigenvalues and configurations. I measured the 100 smallest magnitude eigenvalues of $H_4(m_0)$ at $m_0 = 1.9$ for 110 independent configurations (separated by 20 configurations, i.e. a total of 2200 configurations were generated). The fraction of eigenvalues

with values between λ and $\lambda + d\lambda$ is plotted vs λ in Fig. 5. Here $d\lambda \approx 0.007$. The difference in the distributions is telling. The 0-flavor Wilson distribution has nonzero support at $\lambda = 0$ and is raising almost linearly with a small slope as λ increases. On the other hand, the 2-flavor Wilson distribution has zero support between $\lambda = 0$ and $\lambda = 0.015$. After that it is raising very slowly until $\lambda = 0.05$. It does not exceed the 0-flavor distribution until λ gets larger than ≈ 0.12. Larger statistics are needed to paint a clearer picture. Of course it may be that the distribution has zero support only at $\lambda = 0$ and then it increases perhaps quadratically. Nevertheless the point is that for a numerical simulation of QCD that typically generates a few thousand configurations the method creates a substantial gap.

As discussed, it is expected that the added 2-flavors of Wilson flavors with supercritical mass $\mu = -1.9$ should
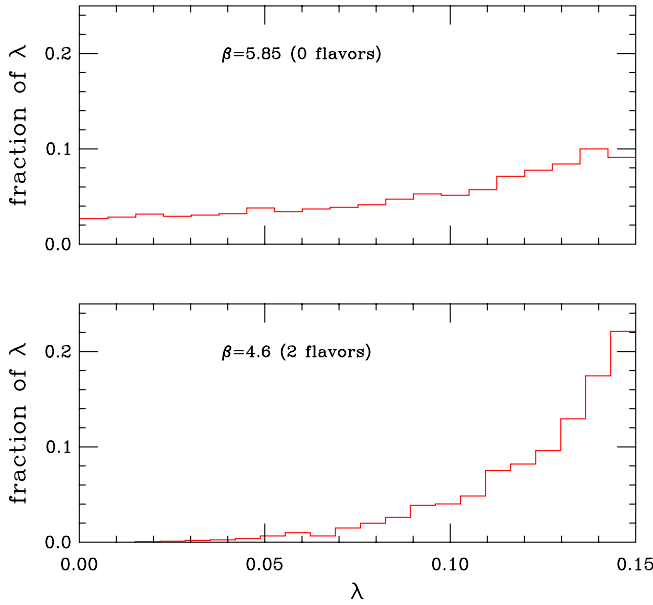
FIG. 5 (color online).   The 100 smallest magnitude eigenvalues of $H_4(m_0)$ at $m_0 = 1.9$ were measured for 110 independent configurations for $\beta = 5.85$ and 0-Wilson flavors and for $\beta = 4.6$ and 2-Wilson flavors. Both have $a^{-1} \approx 1.4$ GeV. The fraction of eigenvalues with values between λ and $\lambda + d\lambda$ is plotted vs λ. Here $d\lambda \approx 0.007$.

have a hadron spectrum above the lattice cutoff. This is verified in Fig. 6. The pion (diamonds), rho (squares), and nucleon (stars) masses vs a^{-1} in GeV measured using 2-flavor dynamical Wilson fermions (both for the propagator and the sea quarks) are shown. The scale is set using the GDWF ρ mass. The straight line marks the cutoff. Masses above that line are above the lattice cutoff. Clearly the Wilson hadron spectrum is above the lattice cutoff. Most importantly the pion mass is very heavy and above the cutoff. This ensures that the added 2-flavors of Wilson fermions do not affect the low energy physics. On the other hand, they clearly affect the physics near the cutoff. For example, they renormalize the value of β. At $a^{-1} \approx 1.4$ GeV, β changes from 5.85 to 4.6. But, of course, this is expected and is of no consequence.

Also, one may worry that the Wilson fermions may break parity since they have mass in the supercritical region. This is obviously not the case as can be seen from Fig. 4 where the corresponding operator $H_4(m_0) = \gamma_5 \not{D}_w(-m_0)$ has no zero eigenvalues at $m_0 = 1.9$. Nevertheless, I measure the expectation value of $\bar{\Psi}\gamma_5\Psi$ for the three lattice spacings used in this work. The results are shown in Fig. 7. Its value is of the order 10^{-6} with an error that is an order of magnitude larger. It is consistent with zero well within the error. Clearly parity is not broken and one is away from the Aoki phase [24].

The residual mass $m_{\rm res}$ is measured using the ratio method (see for example [23]). In Fig. 8 the quenched DWF and GDWF residual masses $m_{\rm res}$ vs L_s at $a^{-1} \approx$
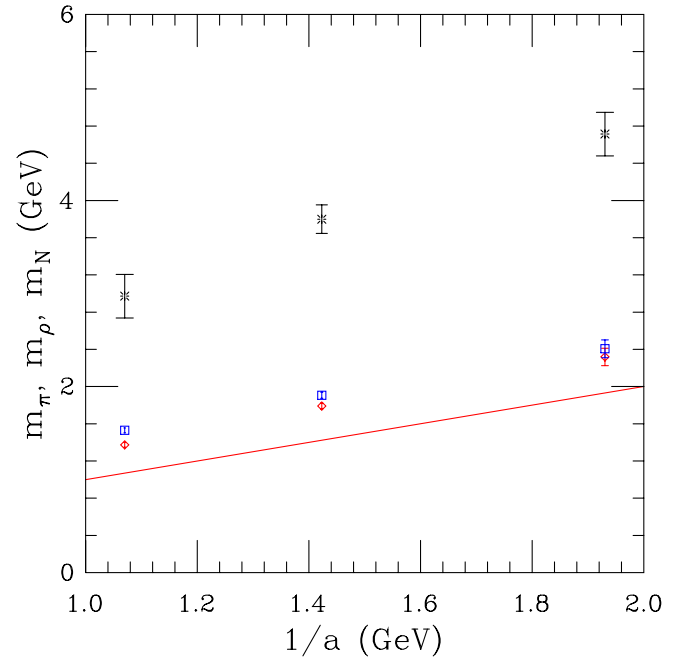

FIG. 6 (color online).   The pion (diamonds), rho (squares), and nucleon (stars) masses vs a^{-1} in GeV measured using 2-flavor dynamical Wilson fermions (both for the propagator and the sea quarks) with mass $\mu = -1.9$. The scale is set using the GDWF rho mass. The straight line marks the cutoff. Masses above that line are above the lattice cutoff.

1.0 GeV are shown. The top points (squares) are from the quenched DWF simulations at $\beta = 5.7$, while the bottom points (diamonds) are from the quenched GDWF
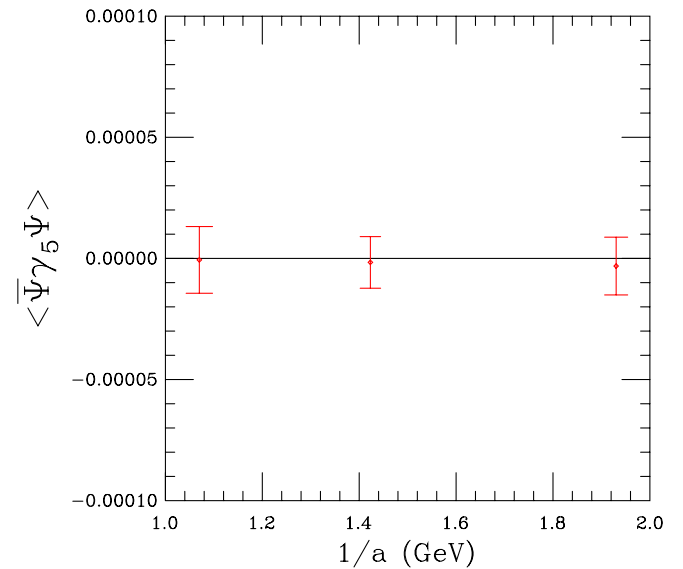

FIG. 7 (color online).   The expectation value of the $\bar{\Psi}\gamma_5\Psi$ condensate in lattice units vs a^{-1} in GeV using 2-flavor dynamical Wilson fermions (both for the propagator and the sea quarks) with mass $\mu = -1.9$. It is consistent with zero well within the error. The lattice spacing is set using the GDWF ρ mass. The straight line marks the y-axis zero line.
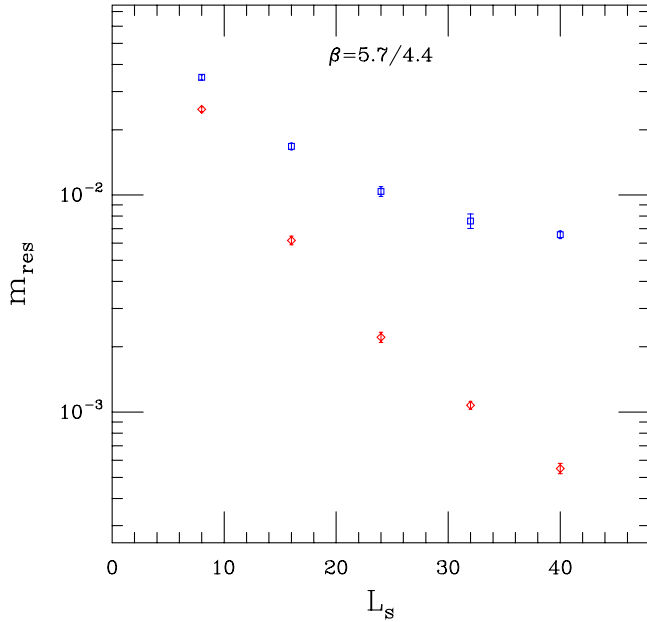
FIG. 8 (color online). The quenched DWF and GDWF residual masses m_{res} vs L_s at $a^{-1} \approx 1.0$ GeV. The top points (squares) are from quenched DWF simulations at $\beta = 5.7$ while the bottom points (diamonds) are from quenched GDWF simulations at $\beta = 4.4$. In both cases $m_0 = 1.9$ and m_{res} was measured at $m_f = 0.02$.

FIG. 9 (color online). The quenched DWF and GDWF residual masses m_{res} vs L_s at $a^{-1} \approx 1.4$ GeV. The top points (squares) are from quenched DWF simulations at $\beta = 5.85$ while the bottom points (diamonds) are from quenched GDWF simulations at $\beta = 4.6$. In both cases $m_0 = 1.9$ and m_{res} was measured at $m_f = 0.02$.

simulations at $\beta = 4.4$. In both cases $m_0 = 1.9$ and m_{res} was measured at $m_f = 0.02$ (the value of m_{res} is fairly insensitive to the value of m_f as can clearly be seen in Fig. 11). The expected faster exponential decay and much smaller values of m_{res} are evident. Already at $L_s = 24$, m_{res} is smaller by almost an order of magnitude. Furthermore, its value $m_{res} \approx 0.002$ is rather nice for such a large lattice spacing. At $L_s = 40$ $m_{res} \approx 0.0005$. The difference becomes more dramatic as the lattice spacing is decreased. The results for $a^{-1} \approx 1.4$ GeV are shown in Fig. 9 and for $a^{-1} \approx 2.0$ GeV are shown in Fig. 10. Figure 9 is most interesting since it corresponds to the lattice spacing of dynamical $N_t = 8$ thermodynamics at the critical temperature. At $L_s = 24$ $m_{res} \approx 0.0006$ and at $L_s = 32$ $m_{res} \approx 0.0002$.

As mentioned above m_{res} is rather insensitive to m_f. This is shown in Fig. 11 for the GDWF simulations at all three values of β.

Regarding chiral symmetry, one of the most telling observables is the pion mass. At the end of the day any improvement method should result to small pion masses. In Fig. 12 the GDWF pion mass squared vs m_f from quenched GDWF simulations is shown. The squares are the measured data points, the straight line is a least χ^2 fit and the star is the $m_f = 0$ extrapolated point. Here $\beta = 4.4$ corresponding to $a^{-1} \approx 1.0$ GeV, $m_0 = 1.9$, and $L_s = 16$. The straight line fit intersects the x-axis at $m_f \approx -0.004$ which is consistent with the value of $m_{res} \approx 0.006$ from
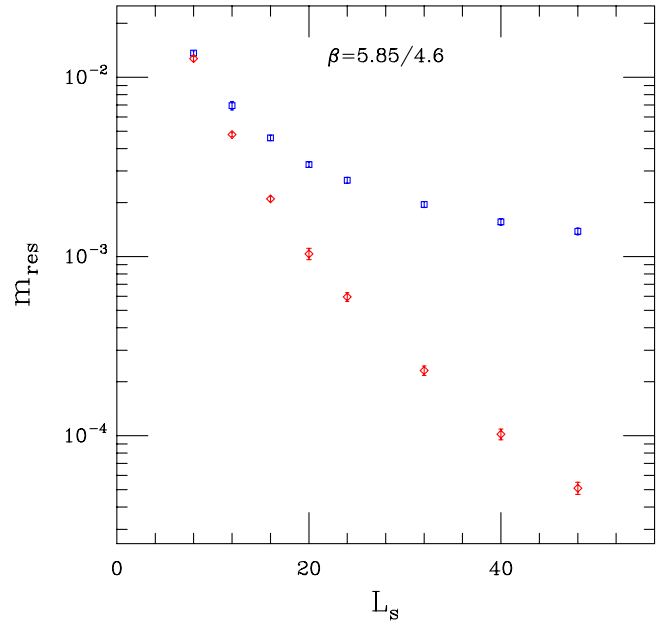

FIG. 10 (color online). The quenched DWF and GDWF residual masses m_{res} vs L_s at $a^{-1} \approx 2.0$ GeV. The top points (squares) are from quenched DWF simulations at $\beta = 6.0$ while the bottom points (diamonds) are from quenched GDWF simulations at $\beta = 4.8$. In both cases $m_0 = 1.9$ and m_{res} was measured at $m_f = 0.02$.
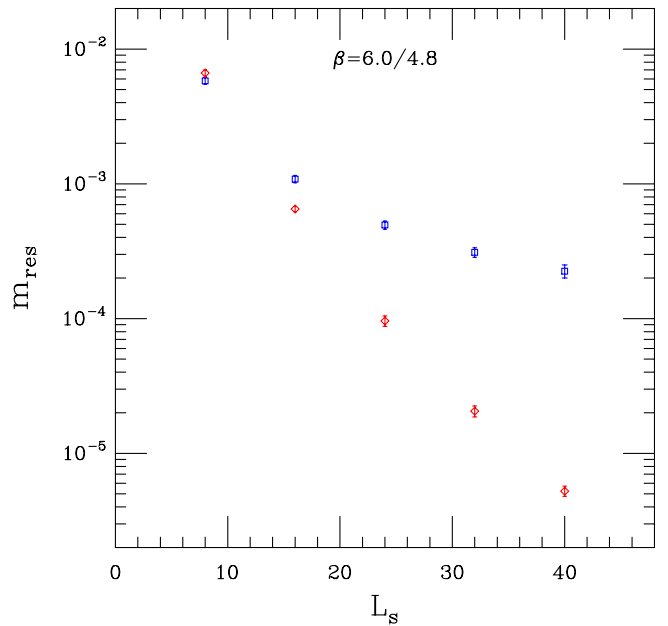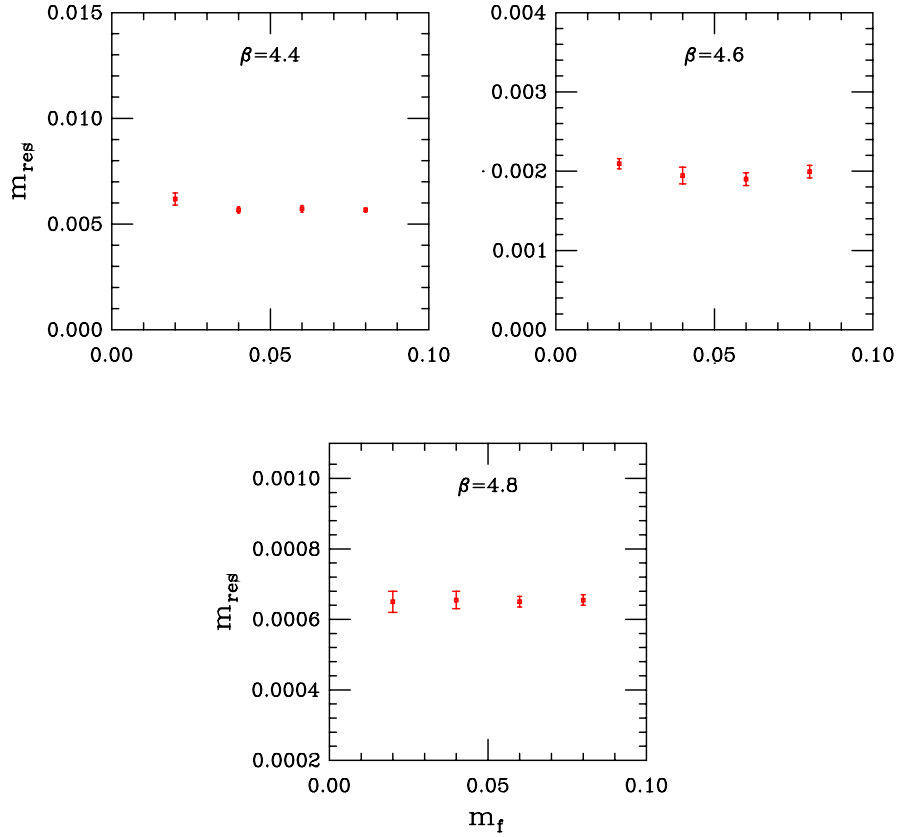
FIG. 11 (color online).   The quenched GDWF residual mass $m_{\rm res}$ vs m_f at $L_s = 16$ for three values of β.

FIG. 12 (color online).   The pion mass squared vs m_f from quenched GDWF simulations. The squares are the measured data points, the straight line is a least χ^2 fit, and the star is the $m_f = 0$ extrapolated point. Here $\beta = 4.4$ corresponding to $a^{-1} \approx 1.0$ GeV, $m_0 = 1.9$, and $L_s = 16$.

FIG. 13 (color online).   The pion mass squared vs m_f from quenched GDWF simulations. The squares are the measured data points, the straight line is a least χ^2 fit, and the star is the $m_f = 0$ extrapolated point. Here $\beta = 4.6$ corresponding to $a^{-1} \approx 1.4$ GeV, $m_0 = 1.9$, and $L_s = 16$.
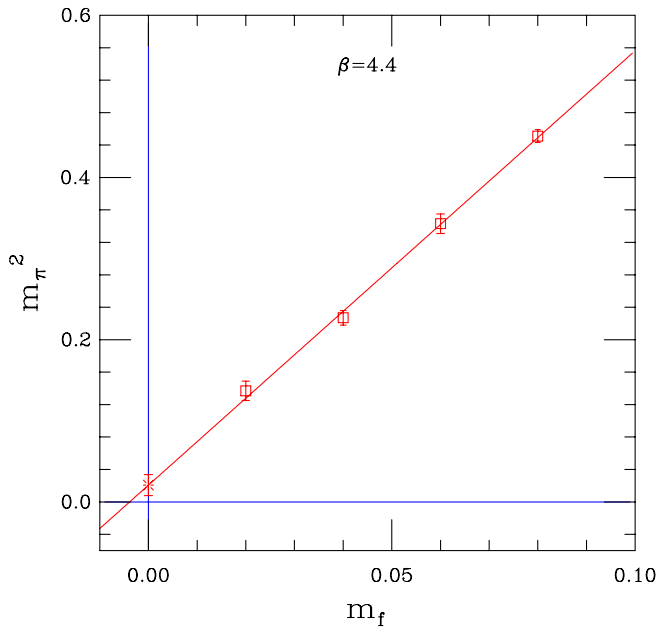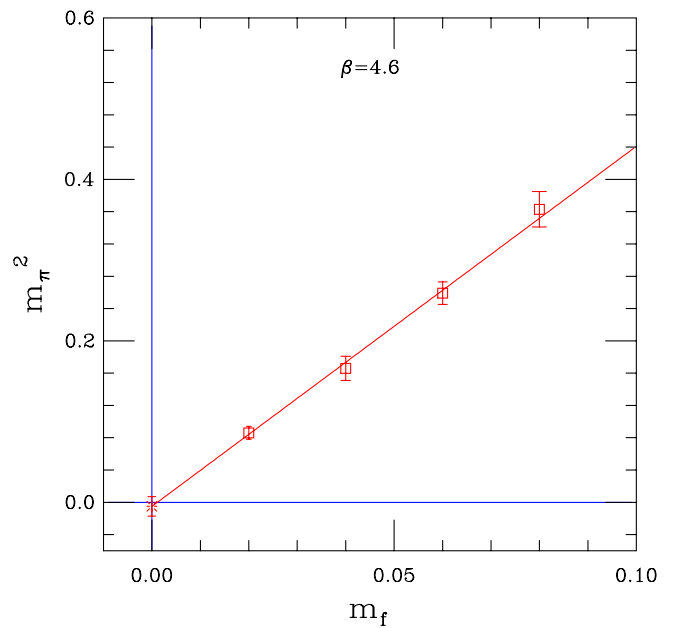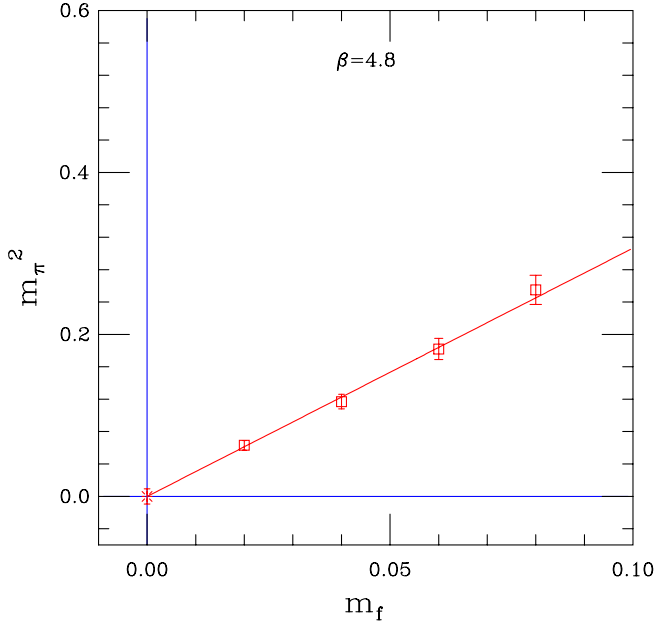
FIG. 14 (color online). The pion mass squared vs m_f from quenched GDWF simulations. The squares are the measured data points, the straight line is a least χ^2 fit, and the star is the $m_f = 0$ extrapolated point. Here $\beta = 4.8$ corresponding to $a^{-1} \approx 2.0$ GeV, $m_0 = 1.9$, and $L_s = 16$.

Fig. 8. The data for $\beta = 4.6$ corresponding to $a^{-1} \approx 1.4$ GeV are shown in Fig. 13 and for $\beta = 4.8$ corresponding to $a^{-1} \approx 2.0$ GeV are shown in Fig. 14. In both cases the straight line fit gives $m_\pi^2 \approx 0$ at $m_f = 0$ within the error bar.

V. LIGHT PIONS IN RUGGED TERRAIN

In this section, I present a simulation of quenched GDWF at $a^{-1} = 1.356(75)$ GeV, $L_s = 24$, and $m_f = 0.005$. The space-time volume is $16^3 \times 32$ and $m_0 = 1.9$. Think of this as the icing on the cake or the cherry on top of the sundae. The point is that this simulation should closely resemble a dynamical GDWF simulation near the $N_t = 8$ critical point of QCD thermodynamics. Also notice that, in order to mimic the way dynamical simulations are analyzed, I calculated the lattice spacing using the ρ mass at the bare quark mass $m_f = 0.005$ and not at the $m_f = 0$ extrapolated value.

I find that $m_{\text{res}} = 0.000\,64(4)$ which is about 10% of the explicit quark mass $m_f = 0.005$. Finally the pion mass is under control. I find $m_\pi = 140(40)$ MeV at $m_f = 0.005$.

VI. TOPOLOGICAL ISSUES

The resolution of the flow diagrams of Fig. 4 does not allow me to measure the net index but does allow me to observe that the number and location of crossings change from configuration to configuration. This indicates the desired instanton anti-instanton activity. Measuring the net index requires more computational resources and is outside the scope of this paper. However, a few remarks are in order.

If the update algorithm "smoothly" transforms the gauge field configuration then the net index will also have to change in a smooth way. In that case the heavy Wilson fermion determinant will prohibit any flow line from crossing through m_0 and as a result the net index will not be able to change. The simulation will generate configurations with the same net index as the initial configuration and will not be able to tunnel between sectors. For example, for an ordered start the net topology will always remain zero. This does not change the ability of the simulation to generate crossings (for example as in Fig. 4). It simply means that the appearance/disappearance of an instanton will always be accompanied by that of an anti-instanton of some size at some location.

Because I could not measure the net index, it is not clear if the HMC Phi algorithm that I used in this work is capable of topologically nonsmooth gauge field evolution that would generate tunneling between sectors. However, this is an algorithmic issue and is not particular to GDWF. For example, net index change is suppressed as the lattice spacing gets smaller irrespectively of using or not using GDWF. The gauge action barriers between topological sectors are a property of QCD. This has not been identified as a problem yet because the couplings used in today's simulations are not weak enough. Even so, algorithms that are able to tunnel between sectors have already been proposed (for example, see [25] and references therein).

Therefore if net index change is important to the physics at hand, one should check the net index properties of HMC Phi under GDWF. If they are not satisfactory then one should use a properly augmented evolution algorithm. In any event, although the subject of net topology is of interest in many cases, one only needs to stay within sector zero provided that the volume is large for the physics at hand. For a very nice investigation on the subject see [26].

VII. ALGORITHMIC AND COMPUTATIONAL COSTS

The algorithmic implementation of a new method is of course a matter of effort and not a matter of concept. However, this effort is not always small. A method that is simple and is easily implemented as an extension of existing methods is highly desirable. This is the case for GDWF. Any QCD code that employs standard DWF or related fermions already has an implementation of the Wilson $\displaystyle{\not{D}}_w(x, x'; \mu)$ operator and evolution force term. Typically one should simply have to add to the DWF force term the Wilson force term and to the corresponding energy function the extra Wilson fermion energy.

The additional computational cost of adding 2-flavors of heavy Wilson fermions to a 2-flavor dynamical DWF simulation is obviously at most an $1/L_s$ fraction. For

example, at $L_s = 24$ it should be less than a $\approx 5\%$ addition to the computation cost.

VIII. CURIOUS THOUGHTS

GDWF bring up a few thoughts that are worthwhile pondering.

Clearly the addition of heavy fermions to the theory is an alteration in the ultraviolet regime. But in the GDWF case it dramatically affects the infrared properties of the theory. After all, this was its purpose. This is an example of physics above the cutoff affecting the physics far below the cutoff. These ''spectator'' fermions may be pointing to some interesting theoretical directions.

GDWF were described as the addition of two extra Wilson fermions with supercritical mass. This leads to a fermionic determinant that directly suppresses the unwanted gauge configurations. In this light, GDWF are simply a device for better simulations of QCD on the lattice. Perhaps there is nothing more to it than that. But it is interesting that GDWF can be interpreted in two additional and different ways.

Another way to think about GDWF is to consider the log of the two-flavor Wilson determinant (with mass $-m_0$) as part of the pure gauge action. As mentioned above it is irrelevant and therefore it is a valid addition to the lattice gauge action. Thinking about it this way opens the method to be applied to the existing wealth of improvement techniques for DWF and related fermions.

Yet another and perhaps most curious way to think of GDWF is to extend the five-dimensional DWF Dirac operator to include two additional diagonal terms along the fifth direction. These terms can be inserted ''behind'' the walls. The determinant of this new Dirac operator is the product of the original DWF determinant times the two-flavor Wilson determinant. More specifically, one will have $L_s + 2$ fermion fields (but still L_s Paulli-Villars fields) and the DWF Dirac operator of Eq. (1) will have to be augmented to the GDWF operator by extending it along the fifth dimension to include two $\not{D}$ terms [see Eq. (2)] along the diagonal. In matrix form on the fifth dimension index the GDWF operator is [for simplicity I have set $m_f = 0$, all blank entries are zero, and $P_{R,L}$ is given in Eq. (4)]

$$
\begin{pmatrix}
\not{D} & & & & & & \\
& \not{D} - 1 & P_R & & & & \\
& P_L & \not{D} - 1 & & & & \\
& & & \ddots & & & \\
& & & & \not{D} - 1 & P_R & \\
& & & & P_L & \not{D} - 1 & \\
& & & & & & \not{D}
\end{pmatrix}.
\tag{8}
$$

In some sense this is a natural extension of DWF. One can think of this as having fermions beyond the walls that do not communicate directly with the fermions inside the walls. Their presence is felt only through their coupling to

the gauge field in the bulk. Notice that the fifth direction midpoint reflection property of DWF is maintained this way. However, also notice that this way one adds two heavy Wilson fermions per DWF flavor. For example, 2-flavor QCD will have an additional four flavors of heavy Wilson fermions. In the numerical simulations of this work, I only used 2-flavors of Wilson fermions. However, using more flavors should not present problems.

IX. OPEN ISSUES

As mentioned earlier, one does not expect dynamical simulations of GDWF to change the quenched results by much, simply because the lattice spacings considered here are large and are the ones of current interest to dynamical simulations. Nevertheless, dynamical tests of GDWF would be very welcomed.

The 2-flavors of Wilson fermions that were added in the action are designed to produce a determinant $\det[H_4]^2$. This suppresses the configurations for which the transfer matrix of DWF has eigenvalue 1. However, H_4 is the transfer matrix Hamiltonian for DWF with a continuous fifth direction. Here I used DWF with a discrete fifth direction. To be sure, the continuous and discrete transfer matrix Hamiltonians have the same zeroes. But the continuous transfer matrix Hamiltonian used here may be more effective for the overlap-Neuberger fermions [13,16] as well as their variants and improvements (see [1–9] and references therein) since it directly relates to them. On the other hand, for DWF with discrete fifth dimension one may want to use instead of a standard Wilson fermion an augmented Wilson fermion that will perhaps further improve the chiral properties of DWF. The exact form of H_4 for the discrete case is known exactly [13,27]. Both of these observations deserve further scrutiny. Furthermore, investigating the applicability of GF to other related fermion regulators [28] is of great interest.

Throughout this work the reader may have been wondering why one should only consider two flavors of Wilson fermions. Why not more? This is indeed a very interesting question deserving further exploration for the obvious extra benefits it may provide in the cost of numerical simulations, but also for purely theoretical reasons. Is a theory with many spectator fermions above the cutoff of any interest?

As mentioned earlier, in production simulations GDWF should be used with improved gauge actions (for example Iwasaki). It is not clear if this will further improve the chiral properties. This certainly deserves more investigation. However, it should be used anyway because it more closely resembles the continuum gauge action.

As discussed in Sec. VI the subject of net-topology change is beyond the scope of this work. However, it is an interesting open issue that needs further investigation. Besides the algorithmic approach discussed in Sec. VI one may want to consider alternative ideas. For example, it has

been proposed that using $\not{D}_w{}^2 + h^2$, where h is a small real number, instead of $\not{D}_w{}^2$ for the two heavy Wilson flavors will produce more frequent net-topology changes as h is increased from zero [1,29]. Clearly h interpolates between GDWF ($h = 0$) and DWF ($h \gg 1$).

Finally, simulations of the $\mathcal{N} = 1$ Super Yang-Mills theory are possible [16,30] and have been performed [11] using DWF. Issues similar to the chiral symmetry of QCD are present and therefore one would expect that GDWF should work there as well. Further exploration is needed.

X. CONCLUSIONS

In this work I demonstrated that the chiral properties of DWF in the large to intermediate lattice spacing a regime of QCD, $1 \text{ GeV} \lesssim a^{-1} \lesssim 2 \text{ GeV}$, are significantly improved by adding to the action two standard Wilson fermions with supercritical mass equal to the negative DWF five-dimensional mass m_0. Here I used $m_0 = 1.9$. I performed quenched DWF simulations and showed that the eigenvalue spectrum of the transfer matrix Hamiltonian develops a substantial *gap* and that the residual mass decreases appreciatively (by about an order of magnitude). I used this key property to name this fermion regulator as GDWF. For other DWF related fermions (for example overlap-Neuberger fermions) I argued that this method of adding ''gap fermions'' (GF) should also improve their chiral properties.

In order to make sure there are no adverse ''side effects,'' I confirmed that local topology changing (measured using the overlap index method) remains active; instantons and anti-instantons with size larger than a lattice spacing are active appearing and disappearing in the gauge field configurations (note that this does not necessarily imply that the net index is changing). Also, I confirmed that the hadron spectrum of the added Wilson fermions is above the lattice cutoff and therefore is irrelevant. Furthermore, I checked that parity is not broken and therefore the added Wilson fermions are well outside the Aoki phase. All numerical simulations in this work were performed on 512-node IBM BlueGene/L supercomputers.

Furthermore, I argued that the results of this work should also hold for dynamical GDWF since I considered rather large lattice spacings which are typical to currently possible dynamical DWF simulations. In particular, the middle of the range of the lattice spacings $1 \text{ GeV} \lesssim a^{-1} \lesssim 2 \text{ GeV}$ approximately corresponds to the $N_t = 8$ critical coupling of the QCD thermal phase transition. This makes the method very appealing for dynamical QCD thermodynamics.

APPENDIX

The evolution in all simulations was done using the standard HMC Phi algorithm. In all cases the trajectory length was set to 0.5. The step size was set to 0.005 or 0.01 depending on the acceptance rate. The acceptance rate in all cases was above 85%. An initial 200 trajectories were used for thermalization. A total of 50 to 100 measurements were done for all propagators. All measurements were separated by 20 trajectories. The conjugate gradient residual was set to 10^{-7}.

The 2-flavor Wilson simulations are obviously full dynamical simulations in the Wilson fermions (they are quenched only with respect to the DWF fermions). The conjugate gradient residual was set to 10^{-6}. The conjugate gradient iterations for the evolution varied between 100 and 200.

All fits in this work including the propagator fits to extract the hadron masses (not shown) had a χ^2 per degree of freedom less than 1.

XI. Tables

The numerical simulation results are presented in the following Tables I, II, III, IV, V, VI, VII, and VIII.

TABLE I. The ρ (m_ρ) and nucleon (m_N) masses in lattice units for quenched GDWF with 2-flavor Wilson fermions, $V = 16^3 \times 32$, $L_s = 16$, and $m_0 = 1.9$. The $m_f = 0.0$ data are from linear extrapolation. Plotted in Fig. 1.

β	m_f	m_ρ	m_N
4.4	0.0	0.720(12)	0.969(23)
4.4	0.02	0.759(10)	1.058(26)
4.4	0.04	0.789(10)	1.115(14)
4.4	0.06	0.815(11)	1.203(14)
4.4	0.08	0.868(10)	1.275(12)
4.6	0.0	0.541(9)	0.712(25)
4.6	0.02	0.596(7)	0.823(22)
4.6	0.04	0.636(19)	0.935(20)
4.6	0.06	0.690(6)	1.036(14)
4.6	0.08	0.753(7)	1.154(15)
4.8	0.0	0.399(16)	0.558(30)
4.8	0.02	0.441(27)	0.640(47)
4.8	0.04	0.522(9)	0.776(19)
4.8	0.06	0.589(7)	0.890(9)
4.8	0.08	0.644(6)	0.993(11)

TABLE II. Matching the scale of quenched GDWF with the scale of quenched DWF. The m_ρ and m_N data are from $m_f = 0$ extrapolations and are in lattice units. The a^{-1} is derived from the GDWF m_ρ mass. The DWF data are from Ref. [23]. The parameters are as in Table I. Plotted in Figs. 2 and 3.

β DWF	β GDWF	m_ρ DWF	m_ρ GDWF	m_N DWF	m_N GDWF	a^{-1} GeV
5.7	4.4	0.756(22)	0.720(12)	1.03(6)	0.969(23)	1.070(18)
5.85	4.6	0.549(14)	0.541(9)	0.74(2)	0.712(25)	1.423(25)
6.0	4.8	0.404(8)	0.399(16)	0.566(21)	0.557(30)	1.930(77)

TABLE III. The m_π, m_ρ, and m_N in GeV measured using 2-flavor dynamical Wilson fermions (both for the propagator and the sea quarks) with mass $\mu = -1.9$ for three values of the lattice spacing. The a^{-1} is derived from the GDWF m_ρ mass and is the same as in Table II. All hadron masses are above the cutoff. Also in the table the expectation value of the Wilson fermion $\bar\Psi\gamma_5\Psi$ condensate is shown in lattice units. It is consistent with zero well within the error. Plotted in Figs. 6 and 7.

a^{-1} GeV	m_π GeV	m_ρ GeV	m_N GeV	$\langle\bar\Psi\gamma_5\Psi\rangle$
1.070(18)	1.373(25)	1.530(26)	2.97(24)	$-0.59(13.77)\times 10^{-6}$
1.423(25)	1.791(31)	1.906(33)	3.80(15)	$-1.65(10.65)\times 10^{-6}$
1.930(77)	2.318(93)	2.406(97)	4.71(23)	$-3.16(11.94)\times 10^{-6}$

TABLE VI. The residual mass m_{res} for quenched DWF and GDWF for various L_s values. The parameters are $V = 16^3 \times 32$, $\beta_{DWF} = 6.0$, $\beta_{GDWF} = 4.8$, $m_0 = 1.9$, and $m_f = 0.02$. Plotted in Fig. 10.

$a^{-1} = 1.930(77)$ GeV		
L_s	m_{res}DWF	m_{res}GDWF
8	0.005 810(345)	0.006 640(405)
16	0.001 085(70)	0.000 650(30)
24	0.000 495(35)	0.000 096 0(85)
32	0.000 310(25)	0.000 020 55(195)
40	0.000 225(25)	0.000 005 25(45)

TABLE IV. The residual mass m_{res} for quenched DWF and GDWF for various L_s values. The parameters are $V = 16^3 \times 32$, $\beta_{DWF} = 5.7$, $\beta_{GDWF} = 4.4$, $m_0 = 1.9$, and $m_f = 0.02$. Plotted in Fig. 8.

$a^{-1} = 1.070(18)$ GeV		
L_s	m_{res}DWF	m_{res}GDWF
8	0.034 860(885)	0.024 820(705)
16	0.016 765(610)	0.006 180(285)
24	0.010 395(545)	0.002 215(120)
32	0.007 595(585)	0.001 075(45)
40	0.006 565(270)	0.000 550(30)

TABLE VII. The quenched GDWF residual mass m_{res} for various values of m_f and for three values of β. The parameters are $V = 16^3 \times 32$, $L_s = 16$ and $m_0 = 1.9$. Plotted in Fig. 11.

m_f	m_{res}, $\beta = 4.4$	m_{res}, $\beta = 4.6$	m_{res}, $\beta = 4.8$
0.02	0.006 180(285)	0.002 095(65)	0.000 650(30)
0.04	0.005 665(145)	0.001 945(105)	0.000 655(25)
0.06	0.005 720(160)	0.001 900(80)	0.000 650(15)
0.08	0.005 665(105)	0.001 995(80)	0.000 655(15)

TABLE V. The residual mass m_{res} for quenched DWF and GDWF for various L_s values. The parameters are $V = 16^3 \times 32$, $\beta_{DWF} = 5.85$, $\beta_{GDWF} = 4.6$, $m_0 = 1.9$, and $m_f = 0.02$. Plotted in Fig. 9.

$a^{-1} = 1.423(25)$ GeV		
L_s	m_{res}DWF	m_{res}GDWF
8	0.013 650(325)	0.012 700(450)
12	0.006 950(385)	0.004 785(115)
16	0.004 585(155)	0.002 095(65)
20	0.003 255(110)	0.001 035(75)
24	0.002 660(100)	0.000 595(34)
32	0.001 950(75)	0.000 231(14)
40	0.001 560(65)	0.000 102(7)
48	0.001 380(60)	0.000 051(4)

TABLE VIII. The quenched GDWF pion mass squared m_π^2 for various values of m_f and for three values of β. The $m_f = 0$ data are from linear extrapolation. The parameters are $V = 16^3 \times 32$, $L_s = 16$ and $m_0 = 1.9$. Plotted in Figs. 12–14.

m_f	m_π^2, $\beta = 4.4$	m_π^2, $\beta = 4.6$	m_π^2, $\beta = 4.8$
0.00	0.021(13)	$-0.005(12)$	$-0.0001(94)$
0.02	0.137(12)	0.086(8)	0.063(6)
0.04	0.227(9)	0.166(15)	0.117(9)
0.06	0.343(12)	0.259(14)	0.182(13)
0.08	0.451(8)	0.363(22)	0.255(18)

[1] P. M. Vranas, hep-lat/0001006.

[2] P. M. Vranas, Nucl. Phys. B, Proc. Suppl. **94**, 177 (2001).

[3] G. T. Fleming, Ph.D. thesis, Columbia University, 2001, hep-lat/0404020.

[4] R. Edwards, Nucl. Phys. B, Proc. Suppl. **106**, 38 (2002).

[5] L. Giusti, Nucl. Phys. B, Proc. Suppl. **119**, 149 (2003).

[6] Ting-Wai Chiu, Nucl. Phys. B, Proc. Suppl. **129**, 135 (2004); M. Golterman and Y. Shamir, Nucl. Phys. B, Proc. Suppl. **129**, 149 (2004).

[7] A. D. Kennedy, Nucl. Phys. B, Proc. Suppl. **140**, 190 (2005).

[8] Robert G. Edwards, Balint Joo, Anthony D. Kennedy, Kostas Orginos, and Urs Wenger, Proc. Sci., LAT2005 (2006) 146 [hep-lat/0510086]; N. Christ, Proc. Sci., LAT2005 (2006) 345, Lattice 2005 Proceedings; N. Cundy, S. Krieg, and Th. Lippert, Proc. Sci., LAT2005 (2006) 107 [hep-lat/0511044].

[9] M. Creutz, hep-lat/0511052; R. G. Edwards *et al.* (LHPC Collaboration), Phys. Rev. Lett. **96**, 052001 (2006).

[10] Hidenori Fukaya, Ph.D. thesis, Kyoto University, 2006, hep-lat/0603008; M. Golterman, Y. Shamir, and B. Svetitsky, Phys. Rev. D **72**, 034501 (2005); **71**, 071502 (2005); M. Golterman and Y. Shamir, Phys. Rev. D **68**, 074501 (2003); K. Nagai and K. Jansen, J. High Energy Phys. 12 (2003) 038; T. Izubuchi and C. Dawson, Nucl. Phys. B, Proc. Suppl. **106**, 748 (2002); P. Hernández, K. Jansen, and M. Lüscher, hep-lat/0007015; Y. Shamir, Phys. Rev. D **59**, 054506 (1999).

[11] G. T. Fleming, J. Kogut, and P. M. Vranas, Phys. Rev. D **64**, 034510 (2001).

[12] D. B. Kaplan, Phys. Lett. B **288**, 342 (1992); Nucl. Phys. B, Proc. Suppl. **30**, 597 (1993).

[13] R. Narayanan and H. Neuberger, Phys. Lett. B **302**, 62 (1993); Phys. Rev. Lett. **71**, 3251 (1993); Nucl. Phys. **B412**, 574 (1994); **B443**, 305 (1995); Patrick Huet, R. Narayanan, and H. Neuberger, Phys. Lett. B **380**, 291 (1996); R. Narayanan and H. Neuberger, Nucl. Phys. **B477**, 521 (1996); Nucl. Phys. B, Proc. Suppl. **53**, 658 (1997); **53**, 661 (1997); Phys. Lett. B **393**, 360 (1997); Y. Kikukawa, R. Narayanan, and H. Neuberger, Phys. Lett. B **399**, 105 (1997).

[14] Y. Shamir, Nucl. Phys. **B406**, 90 (1993); V. Furman and Y. Shamir, Nucl. Phys. **B439**, 54 (1995).

[15] P. M. Vranas, Nucl. Phys. B, Proc. Suppl. **53**, 278 (1997); Phys. Rev. D **57**, 1415 (1998).

[16] H. Neuberger, Phys. Rev. D **57**, 5417 (1998).

[17] R. Edwards, U. Heller, and R. Narayanan, Nucl. Phys. **B522**, 285 (1998); **B535**, 403 (1998); Phys. Lett. B **438**, 96 (1998); Phys. Rev. D **60**, 034502 (1999).

[18] R. Narayanan and P. M. Vranas, Nucl. Phys. **B506**, 373 (1997).

[19] K. G. Wilson, in *New Phenomena in Subnuclear Physics*, edited by A Zichichi (Plenum Press, New York, 1975), Part A, p. 69.

[20] Y. Iwasaki, Nucl. Phys. **B258**, 141 (1985).

[21] Lingling Wu *et al.* (RBC Collaboration), Nucl. Phys. B, Proc. Suppl. **83**, 224 (2000).

[22] L. Levkova and R. Mawhinney, Nucl. Phys. B, Proc. Suppl. **129**, 399 (2004); K. Orginos, Nucl. Phys. B, Proc. Suppl. **106**, 721 (2002); Y. Aoki *et al.*, Phys. Rev. D **69**, 074504 (2004).

[23] T. Blum *et al.* (RBC Collaboration), Phys. Rev. D **69**, 074502 (2004).

[24] S. Aoki, Phys. Rev. D **30**, 2653 (1984).

[25] H. Dilger, Int. J. Mod. Phys. C **6**, 123 (1995); Z. Fodor, S. D. Katz, and K. K. Szabo, J. High Energy Phys. 08 (2004) 003; S. Schaefer and T. DeGrand, Proc. Sci., LAT2005 (2005) 140 [hep-lat/0508025].

[26] H. Leutwyler and A. Smilga, Phys. Rev. D **46**, 5607 (1992).

[27] A. Borici, hep-lat/9912040.

[28] P. Hasenfratz, Nucl. Phys. B, Proc. Suppl. **63**, 53 (1998); T. DeGrand, A. Hasenfratz, P. Hasenfratz, F. Niedermayer, and U. Weise, Nucl. Phys. B, Proc. Suppl. **42**, 67 (1995); P. H. Ginsparg and K. G. Wilson, Phys. Rev. D **25**, 2649 (1982); M. Lüscher, Phys. Lett. B **428**, 342 (1998); R. C. Brower, H. Neff, and K. Orginos, Nucl. Phys. B, Proc. Suppl. **140**, 686 (2005).

[29] N. Christ (private communication).

[30] D. B. Kaplan and M. Schmaltz, Chin. J. Phys. **38**, 543 (2000).